

# Experimental determination of the excitation energy of superdeformed bands in $^{192,194}\text{Hg}$ by analysis of the decay quasicontinuum $\gamma$ rays

T. Lauritsen,<sup>1</sup> T. L. Khoo,<sup>1</sup> I. Ahmad,<sup>1</sup> M. P. Carpenter,<sup>1</sup> R. V. F. Janssens,<sup>1</sup> A. Korichi,<sup>2</sup> A. Lopez-Martens,<sup>4</sup> H. Amro,<sup>1,3</sup> S. Berger,<sup>1</sup> L. Calderin,<sup>1</sup> T. Døssing,<sup>5</sup> S. M. Fischer,<sup>1,\*</sup> G. Hackman,<sup>1</sup> F. Hannachi,<sup>2</sup> C. J. Lister,<sup>1</sup> E. F. Moore,<sup>3</sup> D. T. Nisius,<sup>1,†</sup> C. Schück,<sup>2</sup> and S. Siem<sup>1,6</sup>

<sup>1</sup>Argonne National Laboratory, Argonne, Illinois 60439

<sup>2</sup>C.S.N.S.M, IN2P3-CNRS, bat 104-108, F-91405 Orsay Campus, France

<sup>3</sup>North Carolina State University, Raleigh, North Carolina 27695

<sup>4</sup>ReS F-67037, Strasbourg Cedex 2, France

<sup>5</sup>Niels Bohr Institute, DK-2100 Copenhagen, Denmark

<sup>6</sup>University of Oslo, Oslo, Norway

(Received 29 November 1999; published 19 September 2000)

Superdeformed bands in the mass  $A = 190$  region decay suddenly, over a few states, at relatively low spin and high excitation energy. The decay path is very fragmented and only in a few cases have one-step or two-step decays been seen. Thus, only three superdeformed bands have so far been linked to the normal states they decay to. Most of the  $\gamma$  rays from the decay form an unresolved quasicontinuum spectrum. This paper describes the extraction of the total quasicontinuum decay spectrum that connects the superdeformed and normal yrast states. It also demonstrates that the excitation energy and spins of superdeformed bands can be determined by analyzing this total decay spectrum. The analysis method is first tested in  $^{194}\text{Hg}$ , which is one of the few cases where the excitation energy and spin of the yrast superdeformed band are known, and is then applied to the yrast superdeformed band in  $^{192}\text{Hg}$ , where no one-step decays have been seen thus far.

PACS number(s): 23.20.Lv, 27.80.+w, 23.20.En

## I. INTRODUCTION

Over 175 superdeformed (SD) bands have been found in the  $A = 150$  and  $A = 190$  mass regions [1,2]; yet only three of these are firmly connected to the normal deformed (ND) yrast states by decay paths established from discrete transitions. Thus, fundamental quantities such as *spin*, *parity*, and *excitation energy* have not been experimentally determined for almost all SD bands in these mass regions. In order to address such issues as (i) the magnitude of shell corrections at large deformation, (ii) the origin of identical SD bands, (iii) the mechanisms responsible for the sudden decay-out of the SD bands, and (iv) the description of pairing and level densities in the ND well in the decay-out region, some or all of those quantities must be determined for as many SD bands as possible. It is striking that since the first discovery of one-step decay transitions for band 1 in  $^{194}\text{Hg}$  [3] (late 1995) only a few other cases have been reported [4–6]. This suggests that more than statistics is responsible for the fact that only three bands have been linked so far.

The spectrum of transitions connecting SD and ND states is dominated by unresolved, overlapping  $\gamma$  rays, which form a quasicontinuum (QC) spectrum. At high energy this spectrum contains primary  $\gamma$  rays from the direct decay to low-lying discrete ND levels. The QC spectrum yields the average energy and spin removed in the decay from the SD to the ND states and from these quantities it is possible to deter-

mine the excitation energy and spin of the SD band. This technique is referred to as the “QC method.”

To test how accurately it is possible to determine the excitation energy and spin of a SD band using the QC method, the spectrum following the decay of the yrast SD band in  $^{194}\text{Hg}$  has been extracted and analyzed. The excitation energy, spin, and parity of this band are known [3] and, as a result, the accuracy of the QC method can be evaluated. The QC method is then applied to the ground-state SD band in  $^{192}\text{Hg}$ . This nucleus plays a central role in the  $A = 190$  mass region as most calculations indicate large shell gaps at deformations  $\beta_2 \approx 0.5$  for  $Z = 80$ ,  $N = 112$  [7–10]. Although the band is populated strongly ( $\approx 2\%$  of the total intensity in the nucleus [11,12]), it has proved difficult to establish discrete one-step or two-step pathways linking the band to the ND states. Thus, measuring the excitation energy of this SD band with the QC method is of particular importance.

## II. DECAY-OUT OF SD BANDS: GENERAL CONSIDERATIONS

A SD nucleus trapped in the SD well loses spin and energy by emitting stretched  $E2$  collective  $\gamma$  rays. Because the moment of inertia (MOI) for the SD shape is higher than the MOI of the ND states, the SD states become more excited with respect to the ND yrast line as the decay proceeds. Hence, the SD state is embedded among ND states with growing level density as the spin decreases. Moreover, the intraband transition rates become appreciably smaller at low spin because of the rapid  $E_\gamma^5$  scaling of the transition energies. Thus, as the spin decreases, the admixture of ND states through the barrier separating the ND and SD wells increases

\*Permanent address: Department of Physics, DePaul University, Chicago, IL 60614.

†Permanent address: BIR Inc., Lincolnshire, IL 60069.

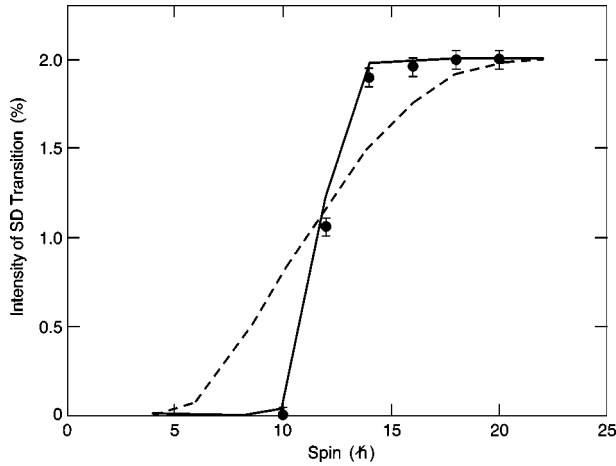


FIG. 1. Calculation of the decay-out from the SD band 1 in  $^{194}\text{Hg}$  using the decay-out theory of Vigezzi *et al.* [14]. The data points are the measured intensities of the SD lines as a function of spin [3]. The solid line shows a calculation where the barrier between the SD and ND well is decreased by  $\approx 25\%$  per  $\hbar$  in the decay-out region (see text for details). The dashed line shows a calculation where the barrier height is kept constant.

significantly, causing decays into the states in the ND well [12–15].

Experimentally, the decay of SD bands is seen to happen suddenly, typically over one to two SD states in the mass 190 region. As a matter of fact, the decay happens faster than one would expect using the decay formalism of Vigezzi *et al.* [14] with a constant SD barrier height. To theoretically reproduce the fast decay, it is necessary to either assume that the SD barrier decreases with spin in the decay-out region or, equivalently, increase the tunneling probability as the spin decreases [14]. Figure 1 shows the calculated intensity of the SD lines during the decay. The data points are the intensities of the SD lines as a function of spin for band 1 in  $^{194}\text{Hg}$ . The solid line is a calculation of the intensities, using the decay-out theory of Vigezzi *et al.* [14], where the height of the barrier between the SD and ND well, 0.95 MeV at spin  $10\hbar$ , is changed by 0.25 MeV per  $\hbar$  of spin (or  $\approx 25\%$ ) in the decay-out region. The SD excitation energy was set to 6.0 MeV (the measured value) at zero spin [3]. The dashed line presents a calculation where the barrier height is constant (and set to 1.6 MeV to ensure that the decay happens near spin  $10\hbar$ ). Clearly, it is necessary to progressively lower the barrier height (or, equivalently, increase the tunneling probability) to reproduce the rapid decay of the SD band. The decrease in the barrier height may be an intrinsic property of the nucleus or it may reflect an increase in the chaoticity of ND states leading to chaos-assisted tunneling [16].

The shape and general characteristics (multiplicity, multipolarity, and intensity distribution) of the QC spectrum are governed by the properties of the admixed levels in the ND well. The end point of the decay spectrum is determined by the excitation energy of the decaying SD state. Thus, because of the high excitation energy at the point of decay, the decay spectrum is expected to be a statistical-like continuum spectrum with some superimposed discrete lines [17], as pointed out in [15]. The decay spectrum is equivalent to that from

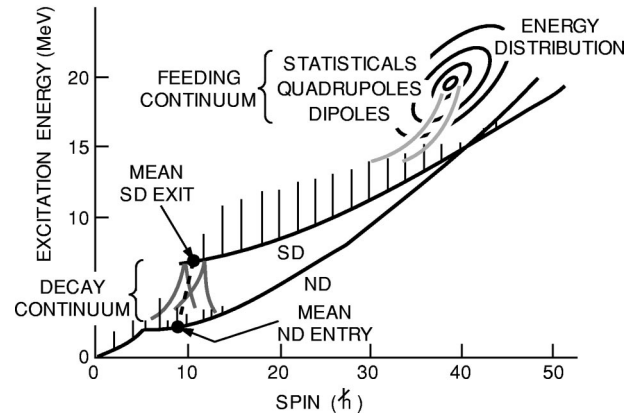


FIG. 2. Schematic diagram of the feeding of ND and SD bands and of the decay of SD bands in the  $A=190$  mass region. Gamma emission starts from the entry distribution. After emission of statistical, quadrupole, and  $M1/E2$  dipole QC  $\gamma$  rays, the deexcitation cascades are trapped either in the ND or SD wells, where discrete  $\gamma$  rays are emitted. If a  $\gamma$  cascade is trapped in the SD well, QC  $\gamma$  rays (as well as some discrete  $\gamma$  rays) are emitted when the SD band decays into the ND states.

neutron-capture states [18]. There are three kinds of discrete lines in the decay spectrum: (i) well-known lines from yrast ND states populated in the decay of the SD bands, (ii) “new” discrete lines from states above the ND yrast line fed in the decay (but not normally populated when the nucleus is fed via ND bands), and (iii) discrete primary  $\gamma$  rays at high energies. The primary  $\gamma$  rays, which represent the first-step transitions to the yrast region, are expected to be subject to large fluctuations in intensity [19,20].

If the discrete primary  $\gamma$  rays at high energies [component (iii)] populate ND states that are either known or can be placed in the ND level scheme, the SD band is said to be linked to the ND states [3–6] and the primary  $\gamma$  rays are called one-step or two-step decay lines (the step refers to the number of  $\gamma$  rays connecting the SD and ND yrast states). Since only three SD bands have been linked in the  $A=190$  region, it appears that the probability for observing such primary decays is small. The case of  $^{194}\text{Hg}$  [3,6] probably represents enhanced primary decays from the tail of the Porter-Thomas distribution [20]. However, in  $^{194}\text{Pb}$  [4,21], the SD band is located at a lower excitation energy. Thus, the phase space for the decay by QC transitions is smaller and this feature enhances the probability for discrete primary transitions. Only in such special cases are these discrete primary  $\gamma$  rays sufficiently intense to be seen with the present generation of  $\gamma$ -detector arrays. It is therefore important to develop other methods to determine the spins and energies of SD levels. Indeed, the quasicontinuum method was developed to take advantage of all components of the decay spectrum to determine two fundamental properties of SD bands: their spins and excitation energies.

### III. PRINCIPLES OF THE QUASICONTINUUM METHOD

The schematic diagram in Fig. 2 illustrates the feeding and decay of a SD band. There are two components to the

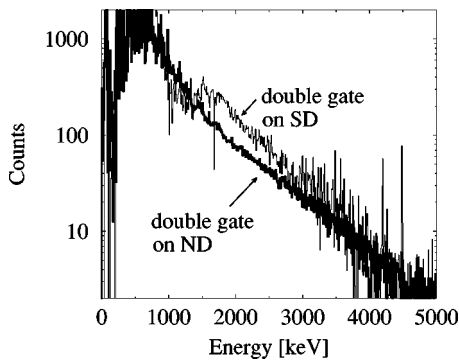


FIG. 3. Comparison of normalized spectra obtained from pairwise coincidence gates on either SD or ND transitions in  $^{194}\text{Hg}$ . The SD spectrum shows additional strength above 1 MeV, from the  $\gamma$  rays associated with the decay of the SD band to the ND states. The spectra were corrected for summing, interactions with neutrons, and are unfolded as described later in the text. The spectra are binned with a resolution of 8 keV/channel. A few peaks, accounting for less than 0.3% of the total multiplicity, are slightly oversubtracted in the energy region from  $\approx 900$  keV to  $\approx 1800$  keV due to small imperfections in the background spectra.

QC: one associated with the feeding of the SD states and the other originating from the decay towards the ND yrast states [13]. A simple way to assess where the decay  $\gamma$  rays are located was illustrated in the work of Henry *et al.* [13], where coincidence spectra gated on ND and SD transitions in  $^{192}\text{Hg}$  were compared. Only the spectra gated on SD  $\gamma$  rays should have an additional decay component from the decay-out to ND levels. Such a comparison for  $^{194}\text{Hg}$  is given in Fig. 3 (with the discrete peaks left in the spectra).

By extracting the total decay spectrum in coincidence with the SD band, it is possible to deduce both the spin and energy of the SD band at the point of decay. When the decay spectrum intensity is normalized to the number of  $\gamma$  cascades, the area of the spectrum determines the average multiplicity, i.e., the average number of steps,  $\bar{m}$ , connecting the yrast SD and ND states. Similarly, the mean energy of the decay spectrum,  $\bar{E}_\gamma$ , determines the average energy removed by these  $\gamma$  rays. Thus, by simple multiplication of these two quantities,

$$\Delta E = \bar{m} \times \bar{E}_\gamma,$$

the mean energy  $\Delta E$  removed by the decay spectrum is established. It is likewise possible to determine the average amount of spin removed by the  $\gamma$  rays:

$$\Delta I = \bar{m} \times \bar{\delta i},$$

where  $\bar{\delta i}$  is the average spin removed by a transition. The latter quantity is calculated using a Monte Carlo simulation of the decay [12]. From the intensities, spins, and energies of the ND transitions in coincidence with the SD band, the average spin and energy corresponding to the entry into the ND levels can be derived (see Fig. 2). By vectorially adding the spin and energy removed by the QC to the mean ND entry point, the *mean exit point* from the SD band can be found.

This exit point is also determined by the decay-out probability and the spins and energies of the SD states. Thus, since the decay-out probability from the SD states can be determined from the in-band transition intensity, the spins and energies of the SD states can be deduced.

An outline of the processing of the data to extract the total decay spectrum in coincidence with the SD band is the following.

(i) Extract clean angle sorted spectra (with no more than a few percent contamination).

(ii) Correct these spectra for the detector response in order to determine the *true* spectra emitted by the nuclei.

(iii) Extract the total QC spectra—which consists of  $\gamma$  rays populating as well as depopulating the SD band.

(iv) Isolate the QC spectra depopulating the SD band.

These steps will be discussed in detail in the following.

#### IV. EXTRACTION OF THE DECAY QUASICONTINUUM IN $^{194}\text{Hg}$

The SD band in  $^{194}\text{Hg}$  was populated with the reaction  $^{150}\text{Nd}(^{48}\text{Ca},4n)$ . Beams were delivered by the 88-Inch Cyclotron at Lawrence Berkeley National Laboratory at an energy of 199 MeV (at midtarget). A combined total of  $5.2 \times 10^9$  triples or higher-fold coincidence events were collected with Gammasphere [22] which at the time comprised 91 high-purity, Compton-suppressed germanium detectors. The total photopeak detector efficiency for  $\gamma$  rays at 1332 keV was about 8%. The target consisted of a  $1.3 \text{ mg/cm}^2$   $^{150}\text{Nd}$  layer evaporated on a thick  $12.4 \text{ mg/cm}^2$  Au backing, which ensured that all  $\gamma$  rays associated with the decay-out of the SD band would be emitted after the nuclei had come to rest in the Au backing [23]. Thus, the primary decay transitions had no Doppler shifts and resulted in sharp lines. A thin  $190 \text{ }\mu\text{g/cm}^2$  layer of Au was evaporated on the front of the target as well to prevent oxidation of the Nd material. Gammasphere was operated in the honeycomb suppression mode to improve the peak-to-total ratio for the  $\gamma$  lines [24]. In this mode, the BGO Compton suppressor shields of neighboring germanium detector modules are used to further suppress Compton-scattered events. This suppression is done in software and the procedure effectively doubles the thickness of the BGO suppressor shields for most detectors. The measured peak-to-total ratio, using a  $^{60}\text{Co}$  source, improved from 0.54 in the standard mode to 0.59 in the honeycomb suppression mode.

In order to extract the decay  $\gamma$  rays from the total spectrum, the data must be processed in a number of steps. Time coincidence gates were applied to each Gammasphere detector in order to create very clean prompt  $\gamma$ -ray spectra. These time gates were made energy dependent in order to take the walk of the timing discriminators into account. In this way, the loss of efficiency at low  $\gamma$ -ray energies, which is customary with large volume germanium detectors, was avoided. Pairwise-coincidence gates were placed on SD transitions in order to obtain SD spectra which were almost free of contaminant coincidences, but yet had sufficient statistics. This was done for each ring of detectors, characterized by a specific polar angle  $\theta$  with respect to the beam direction. Correct

TABLE I. Sources used to determine the response function for Gammasphere. Background spectra were measured and subtracted from the single-line source spectra before the latter were used to determine the response function (see text for details).

Source	$\gamma$ energy [keV]
$^{57}\text{Co}$	122
$^{141}\text{Ce}$	145
$^{139}\text{Ce}$	166
$^{203}\text{Hg}$	279
$^{113}\text{Sn}$	392
$^{85}\text{Sr}$	514
$^{137}\text{Cs}$	662
$^{54}\text{Mn}$	835
$^{65}\text{Zn}$	1116
$^{60}\text{Co}$	1173, 1333
$^{88}\text{Y}$	898, 1836

background subtraction of the double-gated spectra is vital. The Flat Upper Limit (FUL) method [25] was used to subtract peak-background and background-background contributions. The data were also sorted according to the prescription of Ref. [26] in order to avoid “spikes” in the gated spectra. In addition, any lines left in the spectra as a result of contaminant coincidence events (despite careful selection of gates) were identified and characterized before being removed (their contribution to the spectra was typically 1–2 %).

The spectra at each  $\theta$  angle were corrected for the response of the Gammasphere array in a number of successive steps described below. First, the contributions due to coincidence summing of two  $\gamma$  rays were removed following a prescription by Radford *et al.* [27]. The contribution associated with neutron interactions in the Ge detectors (mostly seen in detectors located at forward angles) were subtracted next [28]. This contribution is small (2–3 %) and has minimal impact in the energy region of interest for the QC decay-out  $\gamma$  rays. A very important correction is the removal of the Compton events from the spectra. Even with efficient BGO suppression shields, some Compton events are still present ( $\approx 27\%$ ), and it is necessary to subtract these  $\gamma$  events.

By recording the spectra from one-line and two-line coincidence sources placed at the target position, the response function of Gammasphere was carefully measured. Table I presents the sources used to measure the response of the array. By interpolating between the measured response functions at neighboring discrete energies, the Compton  $\gamma$  rays for the entire spectrum were deduced and subtracted in a manner described in detail in [27] (unfolding technique). Despite the use of energy-dependent gate widths, there was a small reduction in the efficiency at low energy; the response function was corrected for this effect. Figure 4(a) shows a typical spectrum before the unfolding process, together with spectra subtracted during the analysis, i.e., those associated with Compton scattering, neutron interactions, and coincidence summing.

Next, the spectra were corrected for efficiency, all the discrete ND and SD  $\gamma$  peaks below  $\approx 1$  MeV were removed,

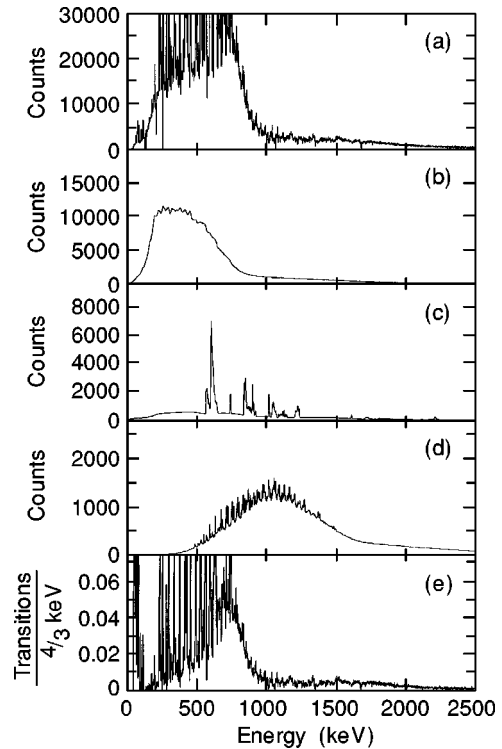


FIG. 4. Measured total spectrum (a) compared with spectra from Compton interactions (b), neutron interactions (c), and summing events (d). Panel (e) shows the spectrum in (a) after the spectra in panels (b)–(d) have been subtracted and after the resulting spectrum has been corrected for efficiency and normalized to transitions per  $4/3$  keV.

and the spectra were contracted to 32 keV/channel. The remaining QC  $\gamma$  rays consist of the three feeding QC components, i.e., statistical, quadrupole, and dipole transitions (from the last step in the feeding [13]), and the decay component. The sought-after decay-out spectrum will be extracted by subtracting the various feeding components. Besides the unresolved components, the decay-out spectrum includes the high-energy one-step and multistep discrete lines.

After corrections for internal conversion and angular distribution, the QC spectra are finally normalized so that the area of the  $2^+ \rightarrow 0^+$  ground-state transition in the spectrum is unity. After this normalization, the integral of the spectrum gives the multiplicity, i.e., the number of steps in the  $\gamma$  cascade. Figure 5 shows the total QC spectrum corrected for angular distribution effects (i.e., the so-called  $A_0$  spectrum).

### A. Statistical feeding component

In Ref. [12], the statistical spectrum feeding the SD band in  $^{192}\text{Hg}$  was calculated, using the experimentally measured entry distribution. This spectrum was calculated with a Monte Carlo code that allows statistical ( $E1$  transitions) and  $E2$   $\gamma$  rays to be emitted in competition in both the SD and ND wells. The  $\gamma$  cascades are started from the measured entry distribution and are followed until they are within 1.2 MeV (on the average) of the yrast line. The formalisms of Vigezzi *et al.* [14] and Bjørnholm and Lynn [29] are incor-

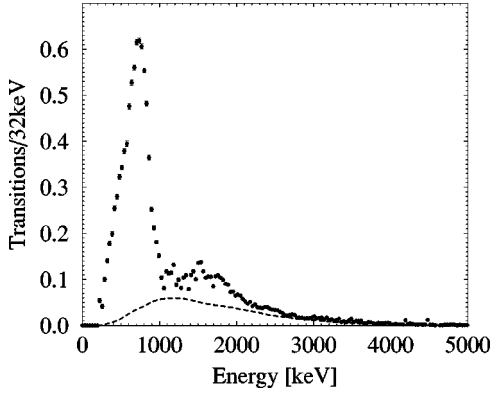


FIG. 5. The efficiency-corrected total QC spectrum (after events due to Compton scattering, neutron interactions, and coincidence summing have been removed). Discrete peaks have also been subtracted. The spectrum is contracted to 32 keV/channel. Also shown is the calculated statistical feeding spectrum (dashed line). (See text for details.)

porated in the Monte Carlo code which also allows for jumps between the ND and SD wells. Trapping in either well occurs when the  $\gamma$  cascades reach the yrast region. The simulation successfully described the feeding of the SD band in  $^{192}\text{Hg}$  [12]. As a matter of fact, this Monte Carlo calculation placed one of the first constraints on the excitation energy of the SD band in  $^{192}\text{Hg}$ —5.2–6.2 MeV at zero angular momentum—by reproducing experimental observables such as the SD band intensity, the SD entry distribution, and the discrete SD-line-intensity profile.

The statistical spectrum calculated in Ref. [12] is also expected to be applicable in the case of  $^{194}\text{Hg}$ . As shown later (see Tables II and III), the measured entry points for the SD bands in the  $^{160}\text{Gd}(^{36}\text{S},4n)^{192}\text{Hg}$  and  $^{150}\text{Nd}(^{48}\text{Ca},4n)^{194}\text{Hg}$  reactions have similar spins and energies above the respective yrast lines. Because the one-step decay lines have been observed in this nucleus [3], it is possible to experimentally confirm that the calculated spectrum is appropriate. The spectrum in coincidence with the one-step lines should contain no other decay-out  $\gamma$  rays, so the only QC  $\gamma$  rays will be those feeding the SD band. Thus, at higher energies (e.g., above the  $E2$  QC  $\gamma$  rays discussed below), it should follow the calculated statistical spectrum. The sum of coincidence spectra, with one coincidence gate placed on one of the one-step decay-out  $\gamma$  rays and a second one on several clean SD lines, has been corrected for the response of Gammasphere. It is presented in Fig. 6, overlaid with the total QC spectrum and the calculated statistical spectrum. Despite the rather low statistics, the agreement between this spectrum and that obtained with double-coincidence gates on SD lines is good beyond the region where the feeding  $E2$   $\gamma$  rays are located. At higher energies, the data are seen to follow the statistical spectrum. Thus, the hypothesis made above is justified. The calculated statistical spectrum is subtracted from the total QC spectrum shown in Fig. 5, thereby eliminating the first of the four QC components. The statistical  $\gamma$  rays are emitted in the early stages of the decay, i.e., while the nucleus has nearly the full recoil velocity. Accordingly, the statistical  $\gamma$  rays are subtracted

TABLE II. Properties of all the feeding and decay spectra in coincidence with the SD band  $^{194}\text{Hg}$ . The feeding components are the statistical, the quadrupole, and the  $M1/E2$   $\gamma$  rays. The decay components are the known ND lines, the “new” ND lines, and the QC  $\gamma$  rays. The sum spin  $\Delta I$  and energy  $\Delta E$  removed in the decay of the SD band establishes the mean SD exit point and the total spin and energy removed by all the components establishes the mean entry point. The mean multiplicities of the individual components are denoted by  $\bar{m}$  and the average energy and spin each  $\gamma$  ray removes are denoted by  $\bar{E}_\gamma$  and  $\bar{\delta i}$ , respectively. The  $A_2$  angular distribution coefficient for the “new” ND lines was found to be  $A_2 = -0.19(5)$ . The mean excitation energy over the SD yrast line at the entry point is 4.2(1.6) MeV.

Component in $^{194}\text{Hg}$	$\bar{m}$	$\bar{E}_\gamma$ (MeV)	$\bar{\delta i}$ ( $\hbar$ )	$\Delta I$ ( $\hbar$ )	$\Delta E$ (MeV)
Statisticals	3.17(16)	1.69(8)	0.66(3)	2.1(2)	5.4(4)
Quadrupoles	4.2(2)	0.73(4)	2.0	8.4(4)	3.1(2)
$M1/E2$ dipoles	3.2(2)	0.55(3)	1.0(3)	3.2(1.0)	1.8(1)
SD lines				28.3(1.4)	7.5(4)
ND lines				9.3(5)	2.4(1)
“New” ND lines	1.4(4)	0.5(1)	1.1(5)	1.5(8)	0.7(2)
QC $\gamma$ rays	2.1(2)	1.7(1)	0.5(1)	1.1(3)	3.7(6)
Decay-out				11.9(1.0)	6.8(5)
Entry point				53.9(2.0)	24.6(1.2)

from the measured spectra of each ring angle, after proper correction for Doppler shift, angular distribution, and relativistic aberrations [30].

### B. Quadrupole feeding component

After the statistical spectrum has been subtracted, the  $A_2$  angular distribution coefficient of the remainder of the spectrum can be found channel by channel: the result is presented in Fig. 7.

If the  $A_2$  coefficient is equal to the measured SD  $E2$  limit of +0.34, the content of the channel is ascribed to be of pure  $E2$  character. Conversely, if the coefficient is equal to the large negative value typical of  $M1/E2$  dipole transitions,

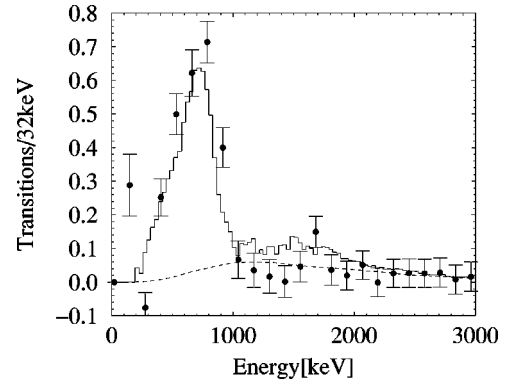


FIG. 6. The QC  $\gamma$  rays obtained from double gates placed on the one-step decay-out lines and SD lines in  $^{194}\text{Hg}$  (data with error bars). Also shown are the total SD spectrum and the calculated statistical spectrum from  $^{192}\text{Hg}$  (dashed line).

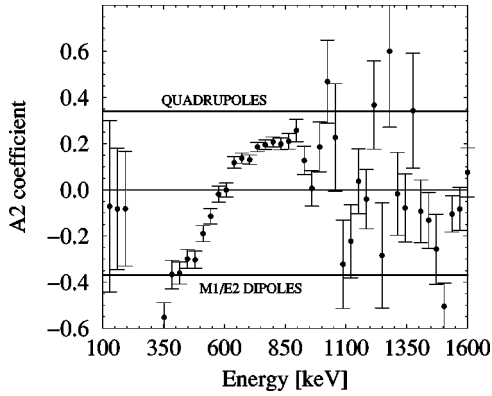


FIG. 7. Angular distribution coefficients, channel by channel, for the QC spectrum after subtraction of the statistical feeding  $\gamma$  rays.

$\approx -0.4$ , the channel content is taken to be of  $M1/E2$  dipole character. (In the analysis, it is assumed that there is no remaining  $E1$  strength in the spectrum below  $\approx 1$  MeV, following the subtraction of the statistical spectrum.) For  $A_2$  coefficients with values between these extremes, the counts in the channels are split proportionally between the two contributions. In this way, the  $E2$  QC component was identified and extracted.

The QC quadrupole  $\gamma$  rays are emitted early in the  $\gamma$  cascade, while the nucleus is still in flight, with a velocity close to the maximum recoil velocity. Hence, the  $A_2$  angular distribution analysis is performed on spectra transformed into the center-of-mass system. The  $E2$  QC component is then subtracted from the laboratory-frame (i.e., measured) spectra of each ring angle, again after proper correction for Doppler shift, angular distribution, and relativistic aberrations.

### C. Decay-out spectrum

After both the statistical and quadrupole components from the feeding have been subtracted, the remaining spectrum consists of (i) the  $M1/E2$  feeding  $\gamma$  rays and (ii) the sought-after decay  $\gamma$  rays (including any one-step and multistep decay lines). There are clear indications of two components in the spectrum in Fig. 8. The low-energy component has large negative  $A_2$  coefficients indicating  $M1/E2$  nature (see Fig. 7) and the upper component resembles the additional strength pointed out earlier from a comparison of the SD- and ND-gated spectra (see Fig. 3). Thus, the upper component ( $\geq 1$  MeV) is assigned to the decay-out process, as it was in Refs. [13,33] for the case of  $^{192}\text{Hg}$ .

As the  $\gamma$  cascades reach the yrast region, new discrete levels above the yrast line will be populated. These “new” levels, which lie above the yrast line, are not normally populated in the decay of ND states and, thus, are not usually included in the known ND level schemes [31]. The decay from these new states will produce discrete  $\gamma$  transitions with energies up to  $\approx 1$  MeV. Figure 9 shows the spectrum of  $\gamma$  rays associated with the decay-out. The data points with error bars are the continuum  $\gamma$  rays above  $\approx 1$  MeV and the new discrete lines are shown below  $\approx 1$  MeV. Table II pre-

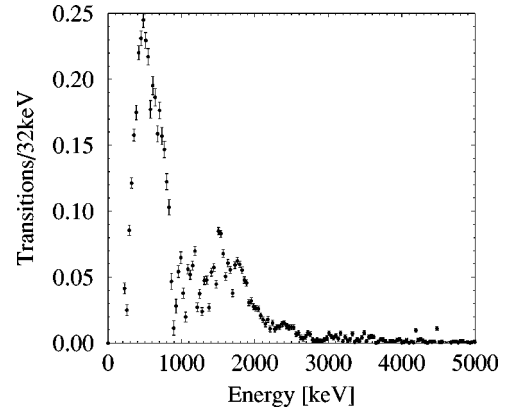


FIG. 8. The QC  $\gamma$  rays in  $^{194}\text{Hg}$  after both the statistical  $\gamma$  rays and the QC of  $E2$  transitions associated with the feeding have been subtracted. The spectrum shows the dipole component of the feeding at low energies ( $\leq 1$  MeV) and the decay  $\gamma$ -ray component at higher energies.

sents the multiplicities and mean energies (as well as other properties) of all the components in coincidence with the SD band in  $^{194}\text{Hg}$ .

### D. Extraction of the energy and spin of the SD band

The decay spectrum from the SD band to the ND states is composed of the two components displayed in Fig. 9: the “new” discrete lines at low energies and the QC  $\gamma$  rays at higher energies.

The mean energy of the QC spectrum is 1.7(1) MeV and its area, i.e., multiplicity, is 2.1(2); see Table II. Therefore, it immediately follows that the QC  $\gamma$  rays remove 3.7(6) MeV of energy. From Monte Carlo simulations [12] of a statistical decay at the proper spin and energy it is found that, on average,  $0.5(1)\hbar$  of spin is removed by each QC  $\gamma$  ray. Thus,  $1.1(3)\hbar$  units of spin are removed, on average, by the QC  $\gamma$  rays.

An angular distribution analysis of the “new” discrete lines shows that their average  $A_2$  coefficient is  $-0.19(5)$ .

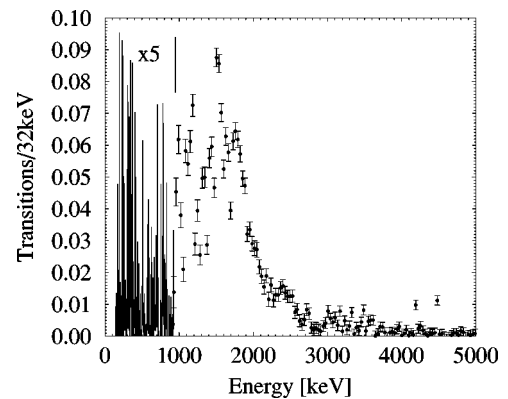


FIG. 9. The extracted  $\gamma$  rays in  $^{194}\text{Hg}$  connecting the SD and ND yrast states. The data points with error bars are the continuum  $\gamma$  rays at energies above  $\approx 1$  MeV (on a scale of transitions/32 keV). The histogrammed data correspond to the spectrum of new discrete lines, scaled by a factor of 5, and are shown with a resolution of 4/3 keV/channel.

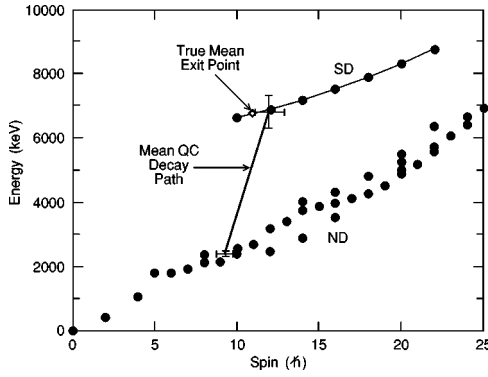


FIG. 10. The mean SD exit point in  $^{194}\text{Hg}$ ,  $11.9(1.0)\hbar$  and  $6.8(5)$  MeV, found by adding the spin and energy removed by known ND lines, new unassigned ND lines, and the decay-out QC  $\gamma$  rays. The true mean SD exit point ( $11.1\hbar$  and  $6.77$  MeV) is deduced from the intensity of the SD band transitions.

Assuming that only stretched  $E2$  and stretched  $E1$  transitions are emitted from the “new” states, it follows that the average spin removed by each “new” line is  $1.1(5)\hbar$ . Thus, the “new” discrete lines remove a total of  $1.5(7)\hbar$  of spin. Likewise, they remove  $0.7(2)$  MeV of energy in the decay-out process.

The spin and energy of the average entry point into the ND yrast line (ND entry point),  $(\langle e \rangle, \langle i \rangle)$ , are found from the equations

$$\langle i \rangle = \sum_i S(i) * \Delta I_\gamma(i), \quad \langle e \rangle = \sum_i S(i) * E_\gamma(i),$$

where  $S(i)$  are the normalized areas of the known ND lines [31] seen in coincidence with the SD band, and  $E_\gamma$  and  $\Delta I_\gamma$  are the energy and spin they remove. In this case, the average entry point into the ND yrast states is at a spin of  $9.3(5)\hbar$  and at an energy of  $2.4(1)$  MeV. The errors quoted here are mostly due to the normalization procedure (to give unit multiplicity for the ground-state transition) and to difficulties of measuring accurately the intensities of low-energy  $\gamma$  rays, which are not observed efficiently with Gammasphere.

By adding all the contributions, i.e., the known ND lines, the new lines just discussed, and the decay-out QC  $\gamma$  rays, the *mean SD exit point* is determined. The result is presented in Fig. 10 and Table II. In the figure, a vector characterizing the mean decay path, obtained as described above, links the average entry point into the ND levels and the SD exit point. It is this SD exit point, located at  $11.9(1.0)\hbar$  and  $6.8(5)$  MeV, that can be compared directly to the result obtained from the exact energy and spin of the SD band—obtained from the decay scheme based on the one-step and two-step decay lines [3,6]. The intensities of the lowest SD transitions are  $I(377 \text{ keV})=100\%$ ,  $I(337 \text{ keV})=99\%$ ,  $I(296 \text{ keV})=95\%$ , and  $I(254 \text{ keV})=53\%$ , respectively. It then follows that the average exit point  $(\langle I \rangle, \langle E \rangle)$  from the band is given by

$$\langle I \rangle = I + 1.06\hbar, \quad \langle E \rangle = E + 0.138 \text{ MeV},$$

where  $I$  and  $E$  are the spin and energy of the state fed by the 254 keV line. The spin and energy of this state were determined by Khoo *et al.* [3] to be  $10\hbar$  and  $6.63$  MeV, respectively, establishing the true mean SD exit point as  $(11.1\hbar, 6.77 \text{ MeV})$ . Thus, the QC analysis reproduces the actual exit point to within  $0.8(1.0)\hbar$  and  $0.0(5)$  MeV.

Alternatively, one can use the QC method to deduce the spin and energy of the  $10^+$  SD state in  $^{194}\text{Hg}$  (i.e., the state fed by the 254 keV line):

$$I = 10.8(1.0)\hbar,$$

$$E = 6.6(5) \text{ MeV}.$$

The excitation energy result is in excellent agreement with that obtained from the decay scheme of Ref. [6]:  $6.6$  MeV. However, the spin of the SD band is somewhat overestimated, although it agrees with the exact result within errors.

## V. EXTRACTION OF THE DECAY SPECTRUM IN $^{192}\text{Hg}$

As stated above, most calculations indicate the presence of large shell gaps at a deformation of  $\beta_2 \approx 0.5$  for  $Z=80$ ,  $N=112$  [1]. Thus,  $^{192}\text{Hg}$  plays a central role in the  $A=190$  SD mass region and it is, therefore, important to establish the excitation energy of the lowest SD band in this nucleus (band 1). No one-step transitions to the ND yrast line have been identified so far and only two tentative two-step decay pathways connecting the SD and ND yrast lines have been proposed [32]. Although several high-energy primary transitions have been detected, Porter-Thomas fluctuations in their strength do not lead to detectable one-step transitions.

The first experimental determination of the excitation energy of the ground-state SD band in  $^{192}\text{Hg}$  was performed with the QC method [13,33]. The data at that time were obtained from early versions of the new  $\gamma$  detector arrays, i.e., with detector systems that were not as powerful as those available today. The present analysis is based on data from Gammasphere in its final configuration and contains significantly higher statistics. Furthermore, the QC analysis techniques have also been improved. Most significantly, the spectra are now treated angle by angle and there is sufficient statistics to allow inspection of individual pairwise gates and the selection of clean ones only. Furthermore, the  $E2$  feeding QC spectrum is now extracted in the center-of-mass frame, and reconstructed in the laboratory frame before subtraction to permit a more accurate extraction of the decay spectrum.

An analysis, completely identical to the one just discussed for SD band 1  $^{194}\text{Hg}$ , was therefore performed for SD band 1 in  $^{192}\text{Hg}$ . The data were collected using the reaction  $^{160}\text{Gd}(^{36}\text{S}, 4n)^{192}\text{Hg}$ . Beams at an energy of  $157$  MeV (mid-target) were delivered by the 88-Inch Cyclotron at Lawrence Berkeley National Laboratory. A total of  $2.1 \times 10^9$  quadruple or higher fold coincidence events were collected with Gammasphere, after prompt coincidence times gates were applied. The target consisted of a  $1.58 \text{ mg/cm}^2$   $^{160}\text{Gd}$  layer evaporated on a thick ( $12.4 \text{ mg/cm}^2$ ) Au backing. At the time, Gammasphere was comprised of 96 Compton-suppressed germanium detectors.

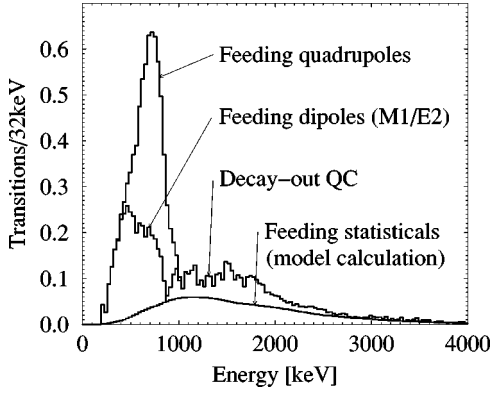


FIG. 11. QC components extracted using the QC method for the yrast SD band in  $^{192}\text{Hg}$ .

Figure 11 presents a combined plot with all the QC components that are in coincidence with the yrast SD band in  $^{192}\text{Hg}$ . Figure 12 compares the total spectra from  $^{192}\text{Hg}$  and  $^{194}\text{Hg}$  after discrete ND and SD lines were subtracted. The spectra from the two SD bands are very similar. Two notable differences, in  $^{194}\text{Hg}$  are (i) stronger one-step lines ( $E_\gamma > 3500$  keV) and (ii) a higher-energy right hand edge of the E2 bump—a consequence of the survival of higher-spin states against fission. Table III gives the multiplicities and mean energies of the feeding and decay components in  $^{192}\text{Hg}$ .

The mean spin and energy at which the SD decay enters the known ND level scheme [31] were found to be

$$\langle i \rangle = 8.0(8)\hbar \quad \langle e \rangle = 2.0(3) \text{ MeV}.$$

This average ND entry point is significantly lower in spin and energy than in the  $^{194}\text{Hg}$  case. Following the procedure described above, the mean exit point for the SD band in  $^{192}\text{Hg}$  is determined to be

$$\langle I \rangle = 10.4(9)\hbar,$$

$$\langle E \rangle = 5.9(5) \text{ MeV}.$$

Based on an analysis of the  $A_0$  spectrum (corrected for angular distribution) with coincidence gates placed on the

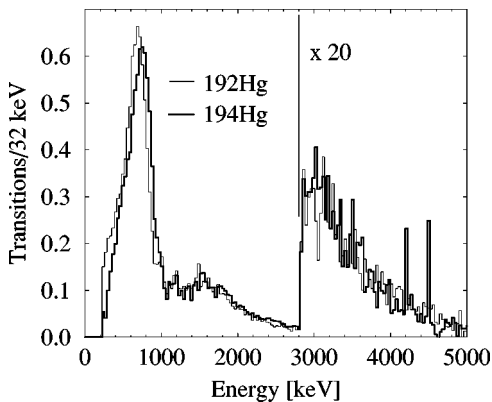


FIG. 12. Spectra from pairwise coincidences of lines from the yrast SD bands in  $^{192,194}\text{Hg}$ .

SD 380 keV line and SD transitions at higher energies, the intensity of the SD transitions at the bottom of the band is found to be  $I(340 \text{ keV}) \equiv 100\%$ ,  $I(300 \text{ keV}) = 91(5)\%$ ,  $I(257 \text{ keV}) = 67(4)\%$ , and  $I(214 \text{ keV}) = 6(1)\%$ . It then follows that the average exit point ( $\langle I \rangle, \langle E \rangle$ ) from the band is given by

$$\langle I \rangle = I + 0.72(23), \quad \langle E \rangle = E + 0.10(3),$$

where  $I$  and  $E$  are the spin and energy of the state fed by the 257 keV line. Hence, the level fed by the 257 keV SD line is determined from this analysis of the decay spectra to have spin and energy

$$I = 9.7(1.0)\hbar,$$

$$E = 5.8(5) \text{ MeV}.$$

Both systematic and statistical errors are included in the quoted errors.

The early analysis of the QC in  $^{192}\text{Hg}$  presented in [13] found the excitation energy at spin  $10\hbar$  to be 6.7(9) MeV which agrees, within errors, with the present result. Using the spin-fit method [34], the spin of the SD level fed by the 257 keV SD line in  $^{192}\text{Hg}$  is evaluated to be  $10\hbar$ , which agrees with the present results within errors.

The relative excitation energy, with respect to the ND yrast line, of SD band 1 in  $^{192}\text{Hg}$  is  $U = 3.3(5)$  MeV (at spin  $10\hbar$ ). In  $^{194}\text{Hg}$ , this relative excitation energy is  $U = 4.2$  MeV. The relative excitation energy of the SD band in  $^{192}\text{Hg}$  is found to be lower than in  $^{194}\text{Hg}$ , confirming trends seen in theoretical calculations [8–10,35,36].

TABLE III. Properties of all the feeding and decay spectra in coincidence with the SD band  $^{192}\text{Hg}$ . The feeding components are the statistical, the quadrupole, and the  $M1/E2$   $\gamma$  rays. The decay components are the known ND lines, the “new” ND lines, and the QC  $\gamma$  rays. The sum spin  $\Delta I$  and energy  $\Delta E$  removed in the decay of the SD band establishes the mean SD exit point and the total spin and energy removed by all the components establishes the mean entry point. The mean multiplicities of the individual components are denoted  $\bar{m}$  and the average energy and spin the  $\gamma$  rays remove are denoted by  $\bar{E}_\gamma$  and  $\bar{\delta i}$ , respectively. The  $A_2$  angular distribution coefficient for the “new” ND lines was found to be  $A_2 = -0.11(6)$  and the mean excitation energy over the SD yrast line at the entry point is 4.6(1.2) MeV.

Component in $^{192}\text{Hg}$	$\bar{m}$	$\bar{E}_\gamma$ (MeV)	$\bar{\delta i}$ ( $\hbar$ )	$\Delta I$ ( $\hbar$ )	$\Delta E$ (MeV)
Statisticals	3.17(16)	1.69(8)	0.66(3)	2.1(2)	5.4(4)
Quadrupoles	5.0(3)	0.68(3)	2.0	10.0(6)	3.4(3)
$M1/E2$ dipoles	2.9(2)	0.47(2)	1.0(3)	2.9(9)	1.4(1)
SD lines				23.3(1.2)	5.7(3)
ND lines				8.0(8)	2.0(3)
“New” ND lines	1.1(3)	0.5(1)	1.2(2)	1.4(4)	0.54(18)
QC $\gamma$ rays	2.2(2)	1.6(1)	0.5(1)	1.1(2)	3.4(4)
Decay-out				10.4(9)	5.9(5)
Entry point				48.7(1.9)	21.8(8)

TABLE IV. Comparison of experimental data and theory predictions of the SD excitation energies  $E_{\text{exc}}^{SD}$  for  $^{192,194}\text{Hg}$  at zero angular momentum. The relative excitation energies for the SD bands in the two nuclei are also shown.

Source	$^{192}\text{Hg } E_{\text{exc}}^{SD}$	$^{194}\text{Hg } E_{\text{exc}}^{SD}$	Difference
Ref. [35] NL1	3.92 MeV	5.6 MeV	1.7 MeV
Ref. [35] NL3	4.46 MeV	6.0 MeV	1.5 MeV
Ref. [36]	5.0 MeV	6.9 MeV	1.9 MeV
Ref. [8]	3.7 MeV	4.6 MeV	0.9 MeV
Ref. [9]	4.2 MeV	5.0 MeV	0.8 MeV
Ref. [10] SkM	4.7 MeV	5.5 MeV	0.8 MeV
Ref. [10] SkP	4.6 MeV	5.5 MeV	0.9 MeV
Ref. [10] SLy4	5.2 MeV	6.5 MeV	1.3 MeV
Experiment	5.3(5) MeV	6.0 MeV	0.7(5) MeV

The SD excitation energies extrapolate to  $E_{\text{exc}}^{SD} = 5.3(5)$  MeV and 6.0 MeV at zero angular momentum for  $^{192,194}\text{Hg}$ , respectively. The extrapolation was performed with a functional form of the excitation energy written as

$$E(I) = E_0 + a[I(I+1)] + b[I(I+1)]^2,$$

where  $E(I)$  is the energy of the SD level at spin  $I$ .

There are several theoretical calculations of the excitation energy of SD bands in this mass region. A sample of these is given in Table IV and compared with experimental results from this work and [3]. None of the calculations reproduces the yrast SD excitation energies in both  $^{192}\text{Hg}$  and  $^{194}\text{Hg}$ . However, all calculations correctly obtain a lower yrast SD energy in  $^{192}\text{Hg}$  and Refs. [8,9], and [10] (with Skyrme forces SkP and SkM) do provide relative excitation energies consistent with the experimental results. In Ref. [10], the two-neutron and two-proton separation energies of the ND and SD ‘‘ground’’ states are also compared. In general, the accuracy of all theories for calculating two-neutron and two-proton separation energies is about 1 MeV.

It should be recognized that the result obtained here for  $^{192}\text{Hg}$  is also in good agreement with the excitation energy constraints of Ref. [12]: 5.2–6.2 MeV at zero angular momentum. The latter result was obtained by the requirement to reproduce, by calculation, all observables connected with the feeding of the SD band in  $^{192}\text{Hg}$ .

## VI. SUMMARY AND FUTURE PROSPECTS

The spectrum from the decay of the superdeformed band 1 in  $^{194}\text{Hg}$  has been extracted and analyzed using the quasicontinuum method. The derived excitation energy of the superdeformed band was found to be in excellent agreement with the exact result determined from one-step and two-step decay lines. This demonstrates the validity of the quasicontinuum method, which can be used to determine the excitation energy of SD bands in instances where one-step or two-step decay lines are not observed. The uncertainty of the method is estimated to be  $\approx 500$  keV, largely governed by systematic uncertainties in the normalization and in subtracting a calculated statistical feeding spectrum. The spin of the SD band is somewhat overestimated although it agrees with the exact result within errors. The uncertainty in the determination of the spin with the quasicontinuum method is  $\approx 1\hbar$ .

The three main uncertainties of the QC method are (i) the calculation of the statistical spectrum, (ii) the normalization of the spectra (in units of multiplicity), and, for the spin determination, (iii) the determination of the spin removed by the QC component and the ‘‘new’’ discrete lines. The quoted errors contain these uncertainties, as well as statistical uncertainties. It follows that the energy determination is more reliable in the quasicontinuum method than the spin determination.

For  $^{192}\text{Hg}$  SD band 1, only weak candidates for two-step decay lines have been seen so far [32]. Thus, the quasicontinuum analysis method was used to determine the spin and energy of this band. Extrapolated to zero angular momentum, the excitation energy of the SD band was found to be 5.3(5) MeV.

No one-step or two-step decay transitions have been found in the mass  $A = 150$  region. Having proved that the quasicontinuum method works well in the  $A = 190$  region, an attempt is currently being made to measure the excitation energy of the superdeformed bands in  $^{151,152}\text{Dy}$  with this approach.

## ACKNOWLEDGMENTS

This work was supported in part by the U.S. Department of Energy, under Contract No. W-31-109-ENG-38.

- [1] R. V. F. Janssens and T. L. Khoo, *Annu. Rev. Nucl. Part. Sci.* **41**, 321 (1991).  
 [2] P. J. Nolan and P. J. Twin, *Annu. Rev. Nucl. Part. Sci.* **38**, 533 (1988).  
 [3] T. L. Khoo, M. P. Carpenter, T. Lauritsen, D. Ackermann, I. Ahmad, D. J. Blumenthal, S. M. Fischer, R. V. F. Janssens, D. Nisius, E. F. Moore, A. Lopez-Martens, T. Dössing, R. Kruecken, S. J. Asztalos, J. A. Becker, L. Bernstein, R. M. Clark, M. A. Deleplanque, R. M. Diamond, P. Fallon, L. P. Farris, F. Hannachi, E. A. Henry, A. Korichi, I. Y. Lee, A. O. Macchiavelli, and F. S. Stephens, *Phys. Rev. Lett.* **76**, 1583

(1996).

- [4] A. Lopez-Martens, F. Hannachi, A. Korichi, C. Schück, E. Gueorguieva, Ch. Vieu, B. Haas, R. Lucas, A. Astier, G. Baldsiefen, M. Carpenter, G. de France, R. Duffait, L. Ducroux, Y. Le Coz, H. Finck, A. Gorgen, H. Hübel, T. L. Khoo, T. Lauritsen, M. Meyer, D. Prevost, N. Redon, C. Rigollet, H. Savajols, J. F. Sharpey-Schafer, O. Stezowski, Ch. Theisen, U. Van Severen, J. P. Vivien, and A. N. Wilson, *Phys. Lett. B* **380**, 18 (1996).  
 [5] D. P. McNabb, J. A. Cizewski, K. Y. Ding, N. Fotiades, D. E. Archer, J. A. Becker, L. A. Bernstein, K. Hauschild, W.

- Younes, R. M. Clark, P. Fallon, I. Y. Lee, A. O. Macchiavelli, and R. W. MacLeod, *Phys. Rev. C* **56**, 2474 (1997).
- [6] G. Hackman, T. L. Khoo, M. P. Carpenter, T. Lauritsen, A. Lopez-Martens, I. J. Calderin, R. V. F. Janssens, D. Ackermann, I. Ahmad, S. Agarwala, D. J. Blumenthal, S. M. Fischer, D. Nisius, P. Reiter, J. Young, H. Amro, E. F. Moore, F. Hannachi, A. Korichi, I. Y. Lee, A. O. Macchiavelli, T. Dössing, and T. Nakatsukasa, *Phys. Rev. Lett.* **79**, 4100 (1997).
- [7] R. R. Chasman, *Phys. Lett. B* **219**, 227 (1989).
- [8] W. Satula, S. Cwiok, W. Nazarewicz, R. Wyss, and A. Johnson, *Nucl. Phys.* **A529**, 289 (1991).
- [9] S. J. Krieger, P. Bonche, M. S. Weiss, J. Meyer, H. Flocard, and P.-H. Heenen, *Nucl. Phys.* **A542**, 43 (1992).
- [10] P.-H. Heenen, J. Dobaczewski, W. Nazarewicz, P. Bonche, and T. L. Khoo, *Phys. Rev. C* **57**, 1719 (1998).
- [11] D. Ye, R. V. F. Janssens, M. P. Carpenter, E. F. Moore, R. R. Chasman, I. Ahmad, K. B. Beard, Ph. Benet, M. W. Drigert, P. B. Fernandez, U. Garg, T. L. Khoo, S. L. Ridley, and F. L. H. Wolfs, *Phys. Rev. C* **41**, R13 (1990).
- [12] T. Lauritsen, Ph. Benet, T. L. Khoo, K. B. Beard, I. Ahmad, M. P. Carpenter, P. J. Daly, M. W. Drigert, U. Garg, P. B. Fernandez, R. V. F. Janssens, E. F. Moore, F. L. H. Wolfs, and D. Ye, *Phys. Rev. Lett.* **69**, 2479 (1992); T. L. Khoo, T. Lauritsen, I. Ahmad, M. P. Carpenter, P. B. Fernandez, R. V. F. Janssens, E. F. Moore, F. L. H. Wolfs, Ph. Benet, P. J. Daly, K. B. Beard, U. Garg, D. Ye, and M. W. Drigert, *Nucl. Phys.* **A557**, 83c (1993).
- [13] R. G. Henry, T. Lauritsen, T. L. Khoo, I. Ahmad, M. P. Carpenter, B. Crowell, T. Dössing, R. V. F. Janssens, F. Hannachi, A. Korichi, C. Schück, F. Azaiez, C. W. Beausang, R. Beraud, C. Bourgeois, R. M. Clark, I. Deloncle, J. Duprat, B. Gall, H. Hübel, M. J. Joyce, M. Kaci, Y. Lecoq, M. Meyer, E. S. Paul, N. Perrin, N. Poffe, M. G. Porquet, N. Redon, H. Sergolle, J. F. Sharpey-Schafer, J. Simpson, A. G. Smith, R. Wadsworth, and P. Willsau, *Phys. Rev. Lett.* **73**, 777 (1994).
- [14] E. Vigezzi, R. A. Broglia, and T. Dössing, *Nucl. Phys.* **A520**, 179c (1990); E. Vigezzi, R. A. Broglia, and T. Dössing, *Phys. Lett. B* **249**, 163 (1990).
- [15] T. L. Khoo, in *Proceedings from the Institute for Nuclear Theory on Tunneling in Complex Systems*, Seattle, WA, 1998, edited by Steven Tomsovic (World Scientific, Singapore, 1998), Vol. 5, p. 229.
- [16] S. Åberg, *Phys. Rev. Lett.* **82**, 299 (1999).
- [17] T. Dössing, T. L. Khoo, T. Lauritsen, I. Ahmad, D. Blumenthal, M. P. Carpenter, B. Crowell, D. Gassmann, R. G. Henry, R. V. F. Janssens, and D. Nisius, *Phys. Rev. Lett.* **75**, 1276 (1995).
- [18] J. E. Lynn, *The Theory of Neutron Resonance Reactions* (Clarendon Press, Oxford, 1968).
- [19] C. E. Porter and R. G. Thomas, *Phys. Rev.* **104**, 483 (1956).
- [20] A. P. Lopez-Martens, T. Dössing, T. L. Khoo, A. Korichi, F. Hannachi, I. J. Calderin, T. Lauritsen, I. Ahmad, M. P. Carpenter, S. M. Fischer, G. Hackman, R. V. F. Janssens, D. Nisius, P. Reiter, H. Amro, and E. F. Moore, *Nucl. Phys.* **A647**, 217 (1999).
- [21] K. Hauschild, L. A. Bernstein, J. A. Becker, D. E. Archer, R. W. Bauer, D. P. McNabb, J. A. Cizewski, K.-Y. Ding, W. Younes, R. Krucken, R. M. Diamond, R. M. Clark, P. Fallon, I.-Y. Lee, A. O. Macchiavelli, R. MacLeod, G. J. Schmid, M. A. Deleplanque, F. S. Stephens, and W. H. Kelly, *Phys. Rev. C* **55**, 2819 (1997).
- [22] I.-Y. Lee, *Nucl. Phys.* **A520**, 641c (1990); P. J. Nolen, F. A. Beck, and D. B. Fossan, *Annu. Rev. Nucl. Part. Sci.* **44**, 561 (1994).
- [23] E. F. Moore, T. Lauritsen, R. V. F. Janssens, T. L. Khoo, D. Ackermann, I. Ahmad, H. Amro, D. Blumenthal, M. P. Carpenter, S. M. Fischer, G. Hackman, D. Nisius, F. Hannachi, A. Lopez-Martens, A. Korichi, S. Asztalos, R. M. Clark, M. A. Deleplanque, R. M. Diamond, P. Fallon, I. Y. Lee, A. O. Macchiavelli, F. S. Stephens, J. A. Becker, L. Bernstein, L. P. Farris, and E. A. Henry, *Phys. Rev. C* **55**, R2150 (1997).
- [24] A. M. Baxter, T. L. Khoo, M. E. Bleich, M. P. Carpenter, I. Ahmad, R. V. F. Janssens, E. F. Moore, I. G. Bearden, J. R. Beene, and I. Y. Lee, *Nucl. Instrum. Methods Phys. Res. A* **317**, 101 (1992).
- [25] B. Crowell, M. P. Carpenter, R. G. Henry, R. V. F. Janssens, T. L. Khoo, T. Lauritsen, and D. Nisius, *Nucl. Instrum. Methods Phys. Res. A* **255**, 575 (1995).
- [26] C. W. Beausang, D. Prevost, M. H. Bergstrom, G. de France, B. Haas, J. C. Lisle, Ch. Theisen, J. Timar, P. J. Twin, and J. N. Wilson, *Nucl. Instrum. Methods Phys. Res. A* **364**, 560 (1995).
- [27] D. C. Radford, R. Holzmann, I. Ahmad, R. V. F. Janssens, and T. L. Khoo, *Nucl. Instrum. Methods Phys. Res. A* **258**, 111 (1987).
- [28] R. Holzmann, I. Ahmad, R. V. F. Janssens, T. L. Khoo, D. C. Radford, M. W. Drigert, and U. Garg, *Nucl. Instrum. Methods Phys. Res. A* **260**, 153 (1987).
- [29] S. Bjørnholm and J. E. Lynn, *Rev. Mod. Phys.* **52**, 725 (1980).
- [30] T. K. Alexander and J. S. Foster, *Advances in Nuclear Physics* (Plenum Press, New York, 1968), p. 197.
- [31] H. Hübel, A. P. Byrne, S. Ogaza, A. E. Stuchbery, G. D. Dracoulis, and M. Guttormsen, *Nucl. Phys.* **A453**, 316 (1986).
- [32] T. L. Khoo (unpublished).
- [33] T. Lauritsen, invited talk, American Chemical Society, Chicago, 1993.
- [34] J. A. Becker, N. Roy, E. A. Henry, M. A. Deleplanque, C. W. Beausang, R. M. Diamond, J. E. Draper, F. S. Stephens, J. A. Cizewski, and M. J. Brinkman, *Phys. Rev. C* **41**, R9 (1990); J. A. Becker, N. Roy, E. A. Henry, S. W. Yates, A. Kuhnert, J. E. Draper, W. Korten, C. W. Beausang, M. A. Deleplanque, R. M. Diamond, F. S. Stephens, W. H. Kelly, F. Azaiez, J. A. Cizewski, and M. J. Brinkman, *Nucl. Phys.* **A520**, 187c (1990); J. E. Draper, F. S. Stephens, M. A. Deleplanque, W. Korten, R. M. Diamond, W. H. Kelly, F. Azaiez, A. O. Macchiavelli, C. W. Beausang, E. C. Rubel, J. A. Becker, N. Roy, E. A. Henry, M. J. Brinkman, A. Kuhnert, and S. W. Yates, *Phys. Rev. C* **42**, R1791 (1990).
- [35] G. A. Lalazissis and P. Ring, *Phys. Lett. B* **427**, 225 (1998).
- [36] J. P. Delaroche, M. Girod, J. Libert, and I. Deloncle, *Phys. Lett. B* **232**, 145 (1989).